water

MDPI

Article

Effects of Orifice Sizes for Uncontrolled Filling Processes in Water Pipelines

Andres M. Aguirre-Mendoza [1,*], Duban A. Paternina-Verona [1], Sebastian Oyuela [2], Oscar E. Coronado-Hernández [1], Mohsen Besharat [3], Vicente S. Fuertes-Miquel [4], Pedro L. Iglesias-Rey [4] and Helena M. Ramos [5]

1 Facultad de Ingeniería, Universidad Tecnológica de Bolívar, Cartagena 131001, Colombia; paterninad@utb.edu.co (D.A.P.-V.); ocoronado@utb.edu.co (O.E.C.-H.)
2 Canal de Experiencias de Arquitectura Naval CEAN, Faculty of Engineering, Universidad de Buenos Aires, Buenos Aires C1063ACV, Argentina; soyuela@fi.uba.ar
3 School of Engineering, Arts, Science and Technology, University of Suffolk at Suffolk New College, Ipswich IP4 1QJ, UK; m.besharat@uos.ac.uk
4 Departamento de Ingeniería Hidráulica y Medio Ambiente, Universitat Politècnica de València, 46022 Valencia, Spain; vfuertes@upv.es (V.S.F.-M.); piglesia@upv.es (P.L.I.-R.)
5 Department of Civil Engineering, Architecture and Georesources, Civil Engineering Research and Innovation for Sustainability (CERIS), Instituto Superior Técnico, University of Lisbon, 1049-001 Lisbon, Portugal; helena.ramos@tecnico.ulisboa.pt
* Correspondence: aguirrea@utb.edu.co

Abstract: The sizing of air valves during the air expulsion phase in rapid filling processes is crucial for design purposes. Mathematical models have been developed to simulate the behaviour of air valves during filling processes for air expulsion, utilising 1D and 2D schemes. These transient events involve the presence of two fluids with different properties and behaviours (water and air). The effect of air valves under scenarios of controlled filling processes has been studied by various authors; however, the analysis of uncontrolled filling processes using air valves has not yet been considered. In this scenario, water columns reach high velocities, causing part of them to close air valves, which generates an additional peak in air pocket pressure patterns. In this research, a two-dimensional computational fluid dynamics model is developed in OpenFOAM software to simulate the studied situations.

Keywords: air valves; computational fluid dynamics; pipeline filling; hydraulic transients

Citation: Aguirre-Mendoza, A.M.; Paternina-Verona, D.A.; Oyuela, S.; Coronado-Hernández, O.E.; Besharat, M.; Fuertes-Miquel, V.S.; Iglesias-Rey, P.L.; Ramos, H.M. Effects of Orifice Sizes for Uncontrolled Filling Processes in Water Pipelines. *Water* **2022**, *14*, 888. https://doi.org/10.3390/w14060888

Academic Editor: Chin H Wu

Received: 14 February 2022
Accepted: 10 March 2022
Published: 12 March 2022

1. Introduction

Filling processes are periodically carried out in water systems after line repairs and maintenance actions that require pipelines to be drained [1]. The air inside the empty pipe can easily be surrounded by the filling fluid, forming a two-phase flow composed of water and air phases. Since air is highly compressible, it is susceptible to generating very high peaks in pressure in interactions with water. During these operations, it is important to consider the modelling of the air–water interaction to prevent the risk of pipeline collapse, since these two fluids exhibit a hydraulic–thermodynamic behaviour [2]. A possible solution for this is the installation of air valves at high points of the piping systems to expel a sufficient quantity of air and avoid high values of air pocket pressure. Several aspects must be considered when dealing with an air venting system. Air valves provide considerable protection for the structural integrity of the piping system [3]. Although air valves are able to improve the system efficiency by preventing air accumulation, they must not be installed blindly, as they can make the situation worse [4]. Air valves can be classified into different types, with air-release valves (ARVs) being the most common type for expelling pressurised accumulated air. ARVs automatically expel accumulated air at sonic velocity, traditionally at high points of pipeline profiles. According to [3], the orifice

diameters of ARVs range from 1 to 5 mm. However, the M51 manual introduces ARVs having diameters ranging from 1.6 to 25 mm [1]. In general, the orifices of ARVs are much smaller than those of other types of air valves.

Many authors have developed one-dimensional (1D) and two- and three-dimensional (2D/3D) computational fluid dynamics (CFD) models to represent the analysis of two-phase operations in water pipelines. The 1D models most widely used in the literature are rigid column [2,5,6] and elastic column models [7–9]. These 1D models consider an air–water interface perpendicular to the main pipe direction. In addition, 2D CFD models have been implemented to study draining operations with different configurations of water pipelines [10,11]. Moreover, 3D CFD models have been used to model the behaviour of filling processes in water installations [12,13]. The authors of [14,15] studied the effects generated by commercial air valves during filling processes, considering pipelines of irregular profile. These investigations are focused on rigid water column formulations. Currently, 2D and 3D CFD models developed for simulating the hydraulic transients generated in filling operations with air valves are scarce in the literature. The authors in [16,17] developed 2D CFD models where the impact of backflow air was studied under different experimental conditions. Additionally, these authors analysed the drainage in pipes with entrapped air, comparing pressure patterns with measurements made by other authors and showing the effects of the length of the entrapped air pocket. The authors of [11] developed a 2D CFD model representing the drainage of an undulate pipeline with trapped air, which was compared with numerical results from a mathematical model in [18] associated with the case. Furthermore, the authors in [19] developed a 2D CFD model to simulate the drainage in an undulate pipeline using an approximation of the geometric aspect ratio to represent the behaviour of air valves. There are several manuals and guidelines to help with the safe operation of pressurised systems containing air pockets. In this context, water distribution companies should execute filling operations considering the recommendations suggested in [1] or other internal practices related to controlling the maximum water velocity (e.g., 0.3 m/s) and the pressure differential (e.g., 13.79 kPa), in order to ensure a controlled operation. The basis for recommendations like these is the need to carry out slow filling for air to have enough time to be expelled. Nevertheless, the risk always exists of rapid filling that can generate severe pressure spikes. This phenomenon has been studied extensively [20–22], but there are still some aspects that need to be explored in more detail.

This research focuses on the analysis of uncontrolled filling operations, which are characterised by the generation of two peaks in air pocket pressure, where the second peak can reach higher values than the first. A 2D CFD model was used to understand the phenomenon, which has the advantage of illustrating the effect of air–water interactions during the generation of overpressure peaks and verifying the velocity gradients generated in the contained air exhaust and in the water column, together with the pressure variation at different points in the hydraulic system. An undulate pipeline profile 7.30 m long with an internal diameter of 51.4 mm was used to validate the results. The uncontrolled filling operations took place when an air-venting orifice of 7.0 mm had been provided for air expulsion purposes. To show the difference between uncontrolled and controlled filling operations, an air valve with an orifice size of 3.175 mm was also used.

2. Experimental Model

The experimental setup consisted of a 7.3 m long undulate PVC pipe with a 51.4 mm internal diameter. The pipeline length was composed of four pipe branches: two horizontal branches with a length of 2.05 m and two inclined branches (constructing a 30° angle with the horizon) with a length of 1.50 m. A hydro-pneumatic tank was used to generate the initial pressure head. In addition, an air-venting orifice with an internal diameter of 7.0 mm was configured for air expulsion purposes (Figure 1). Air pocket pressure oscillations were recorded using a pressure transducer located at the highest point of the piping system. The filling operation was performed using an electro- pneumatic (EP) PVC-U +GF+ ball valve type 230 (Georg Fischer Piping Systems Ltd., Schaffhausen, Switzerland). The EP

valve could open fully in 0.2 s. The EP valve was opened to perform the filling process, for the orifice discharge case. To represent the rapid water filling, the initial pressure was set in the hydro-pneumatic tank to represent various scenarios. The EP valve opened completely in 0.2 s to start the filling process. The entrapped air was expelled from the system pipe via the orifice discharge. The right water column remained at rest during the experimental tests. The pressure transducer recorded variations in air pocket pressure during the experimental procedure. Three (3) experimental tests were conducted in this study, considering different initial hydro-pneumatic pressure heads (P_i/γ_w) with values in the range of 5.10 to 7.65 m.wc, and different air pocket sizes (X_0) in the range of 0.96 to 1.36 m. The orifice size of 7.00 mm was used for all experimental tests (Table 1).

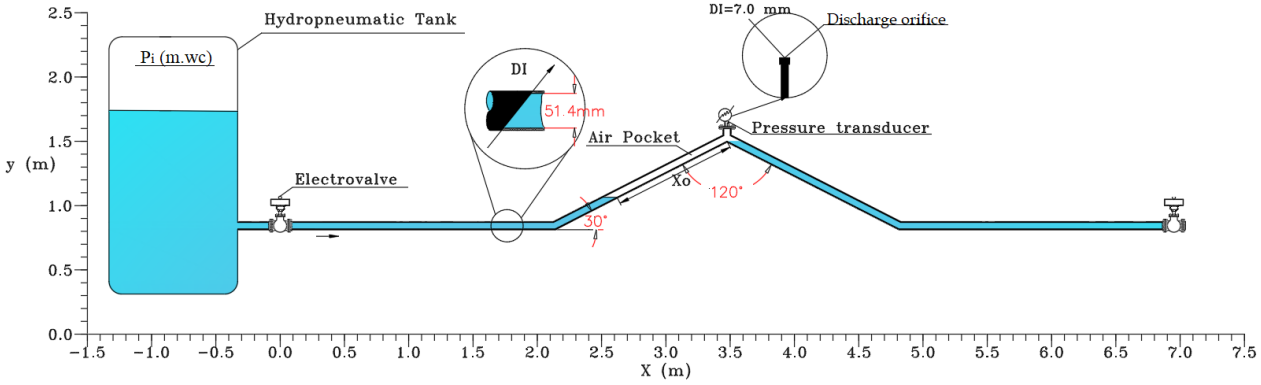

Figure 1. Conceptual scheme of the experimental facility.

Table 1. Test characteristics.

Test	1	2	3
P_i/γ_w (m.wc)	5.10	5.10	7.65
X_0 (m)	0.96	1.36	0.96

3. Numerical CFD Model

3.1. Governing Equations

The governing equations of a multiphase fluid are based on the Navier–Stokes formulations, with the modelling of fluids as a continuous medium. Variations of absolute pressure head and shear forces are evaluated using a finite element analysis, where each cell volume contains information on absolute pressure, temperature, kinetic energy, and fluid density and viscosity.

The Navier–Stokes formulations are composed of continuity and momentum conservation equations. The continuity equation represents the fluid behaviour using X-Y-Z axes, and the momentum conservation equation represents Newton's second law, which is defined using convective, diffusive, viscous, gravitational, and pressure terms:

$$\nabla \cdot (\rho \mathbf{u}) = 0 \tag{1}$$

$$\frac{\partial(\rho \mathbf{u})}{\partial t} + \nabla \cdot (\rho \mathbf{u}\mathbf{u}) = -\nabla p + \nabla \cdot [\mu(\nabla \mathbf{u} + \nabla \mathbf{u}^{\mathbf{T}})] + \rho \mathbf{g} \tag{2}$$

where ρ is the mixture density in the studied cell, $\mathbf{u}$ is the velocity vector of the fluid, p is the absolute pressure, μ is the dynamic viscosity, and $\mathbf{g}$ is the gravitational acceleration vector. The density and dynamic viscosity are functions of the air–water volume fraction (γ). When $\gamma = 0$, then the cell is occupied by air, a value of $\gamma = 1$ represents the condition where the cell is filled with water, and intermediate values of γ represent a mixture of two fluids. Equations (3) and (4) represent the mixture density and dynamic viscosity.

$$\rho = \gamma\rho_w + (1-\gamma)\rho_a \tag{3}$$

$$\mu = \gamma\mu_w + (1-\gamma)\mu_a \tag{4}$$

where subscripts a and w correspond to the air and water phases, respectively. To determine the state of the interface between air and water, an equation for γ is added.

$$\frac{\partial\gamma}{\partial t} + \nabla\cdot(\gamma\mathbf{u}) = 0 \tag{5}$$

3.2. Turbulence Model

In the present investigation, the k-ω SST turbulence model [23] was used, which is suitable for representing a near-wall shear stress distribution characteristic of the two-equation standard k-ω turbulence model in [24] and has a low sensitivity to the vorticity of turbulence events, which can be predicted by the k-ϵ turbulence model in [25]. Furthermore, the model is able to represent the adverse pressure gradients generated by the aerodynamic flows that occur during air expulsion in filling operations. Additionally, the k-ω SST model allows the representation of a logarithmic velocity distribution profile in the boundary layer zone, where the velocity gradient is most sensitive. Viscosity plays an important role in the shear stresses and in the generation of the boundary layer, which allows the adequate representation of the dissipation frequency values at the pipe walls as a function of the fluid conditions in the near-wall zone cells. Equations (6) and (7) show the turbulence model equations:

$$\frac{\partial(\rho k)}{\partial t} + \frac{\partial(\rho u_i k)}{\partial t} = P_k - \beta^*\rho k\omega + \frac{\partial}{\partial x_i}[(\mu + \sigma_k\mu_t)\frac{\partial k}{\partial x_i}] \tag{6}$$

$$\frac{\partial(\rho\omega)}{\partial t} + \frac{\partial(\rho u_i\omega)}{\partial t} = \alpha\frac{1}{\nu_t}P_k - \beta\rho\omega^2 + \frac{\partial}{\partial x_i}[(\mu + \sigma_\omega\mu_t)\frac{\partial\omega}{\partial x_i}] + 2(1-F_1)\rho\sigma_{w2}\frac{1}{\omega}\frac{\partial k}{\partial x_i}\frac{\partial\omega}{\partial x_i} \tag{7}$$

where k is the turbulence kinetic energy, ω is the dissipation frequency, P_k is the shear stress, F_1 is a blending function, u_i is the velocity component, ν_t and μ_t are the turbulent kinematic and dynamic viscosities, respectively, and the remaining variables such as α, β, σ_k and σ_ω associated with the model are defined in [23].

3.3. Assumptions, Boundary Conditions and Mesh Properties

The 2D CFD model simulation was characterised by the low computational expense required for its development. It allowed the simulation of fluids in a two-dimensional domain, where the flow profile is considered to have interactions in the horizontal (X-axis) and vertical (Y-axis) directions. Several researchers have obtained excellent numerical and qualitative results using 2D CFD models to simulate air–water interactions in pipes [10,11,16,17,19].

The 2D CFD simulations were performed using OpenFOAM [26,27], which is a multiphase solver for mixtures of different fluids or phases. The 2D CFD model was used to represent the interaction between two fluids (water and air) in two phases (liquid and gas), which is a situation generated during a filling process with a discharge orifice. The assumptions of the model are:

- The air phase is simulated considering an ideal gas law.
- Fluids are considered compressible, non-isothermal, and immiscible.

The section width of the geometric domain corresponds to the pipe inner diameter (51.4 mm). The initial absolute pressure is supplied by the hydro-pneumatic tank.

A structured mesh was used to guarantee adequate convergence of the solution and to reduce computational time. A dynamic mesh was defined to represent the electro-pneumatic valve opening manoeuvre. A geometric aspect ratio was used to simulate the discharge orifice [19]. Figure 2 shows the considered mesh for the discharge orifice.

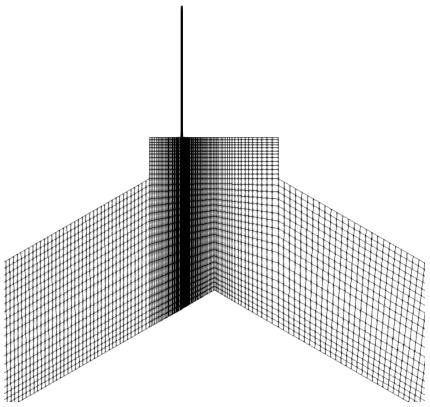

Figure 2. Mesh of the upper end of the irregular pipe with detail in discharge duct.

The geometrical domain presents the following boundaries: (i) an inlet condition governed by the initial absolute pressure of the hydro-pneumatic tank; and (ii) an outlet boundary condition imposed by the atmospheric absolute pressure (101,325 Pa) and the discharge orifice characterisation. A no-split condition was defined at the top and bottom of pipe walls. An initial temperature of 293 K (20 °C) was considered for all simulations. The dynamic mesh was controlled using angular motion data as a function of time. Figure 3 shows the composition of the geometric domain, mesh conditions, and boundaries.

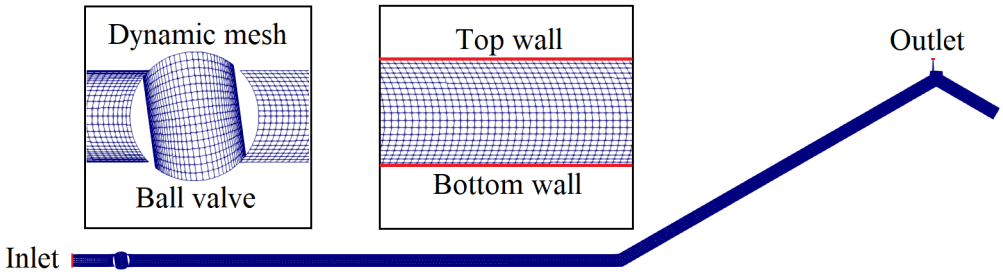

Figure 3. Geometric domain, mesh, and boundary conditions of the pipeline.

The numerical resolution was performed using the PIMPLE algorithm, which is a combination of PISO (pressure implicit with splitting of operator) and SIMPLE (semi-implicit method for pressure-linked equations). The Gaussian quadrature method was used for the calculation of the divergence terms in the 2D CFD model, with second-order and unbounded methods. The backward Euler method was used to represent hydraulic transients, which were implicitly first order and bounded for the temporal scheme. For the execution of the numerical models, the geometric agglomerated algebraic multigrid (GAMG) solver was used to solve the pressure term, with a tolerance during iterative processes of 10^{-6} and a maximum of 20 iterations. In addition, the smooth solver allows the velocity, temperature, turbulent kinetic energy, and dissipation frequency terms to be solved by applying the iterative Gauss–Seidel method, with a maximum tolerance of 10^{-6}. These tolerances are adequate to ensure convergence during the numerical resolution.

4. Results and Discussion

The influence of the discharge orifice size of 7.00 mm was analysed under different initial absolute pressures and air pocket sizes during rapid filling occurrences. The results showed that the 2D CFD model could simulate the detection of two absolute pressure peaks during the experimental tests. A comparison between the calculated and measured absolute pressure patterns is shown in Figure 4.

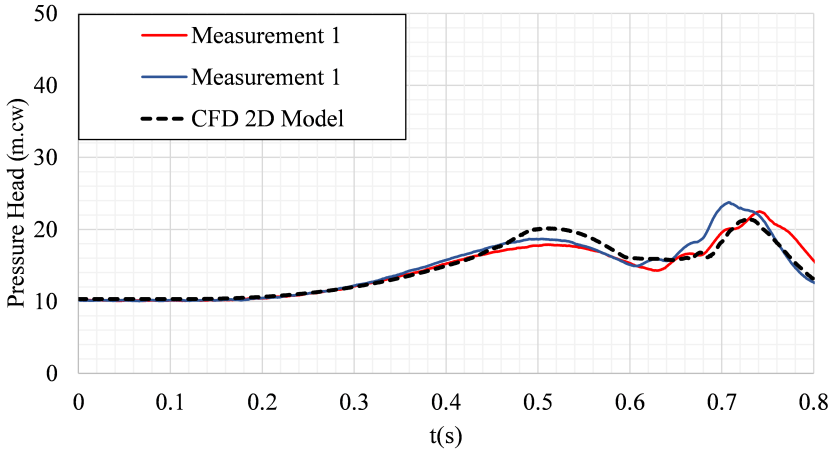

(**a**) Test 1

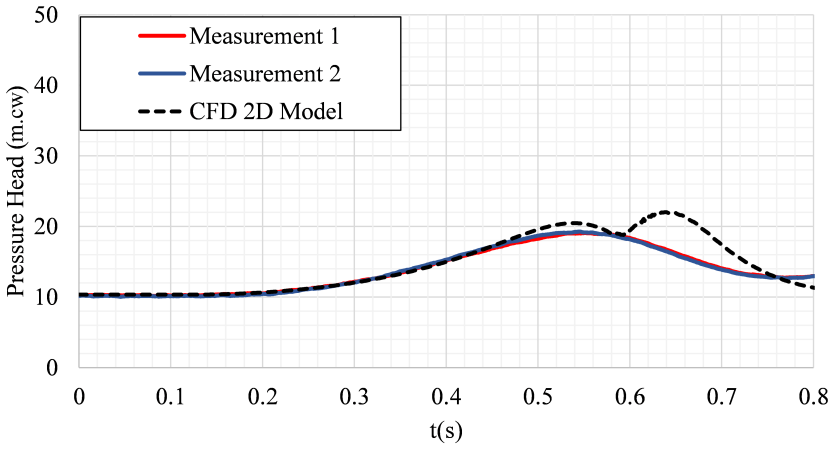

(**b**) Test 2

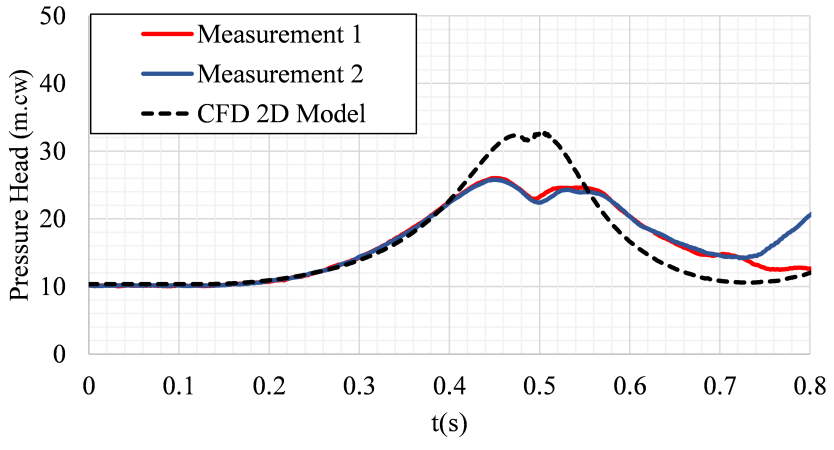

(**c**) Test 3

Figure 4. Comparison between measured and computed air pocket pressure patterns.

Figure 4a shows the air pocket pressure patterns of experimental test 1, where two absolute pressure peaks are generated at 0.51 and 0.74 s, with peak values of 20.14 and 21.52 m.cw, respectively. The second peak in the air pocket pressure pattern is higher than the first. This situation is important because, when considering initial conditions and different pipeline configurations, the higher peak would be used for design purposes. It is important to remember that in a controlled filling process (with standard air valves), the air

pressure fluctuation involves only one pressure peak. A calibration process was used to understand the phenomenon where a secondary peak in the air pocket pressure patterns is observed, since part of the left water column closes the 7.0 mm discharge orifice. It is important to highlight the fact that this phenomenon has not previously been reported in the literature.

Experimental tests 2 and 3 (see Figure 4b,c) were used to validate the 2D CFD model. The results of the validation process showed a small discrepancy between the measured and computed air pocket pressure-head values. For instance, the first peak in experimental test 3 occurred at 0.45 s with an air pocket pressure value of 25.77 m.cw (obtained from the experimental data), which is lower than the value of 32.31 m.cw computed by the 2D CFD model. In the second peak (at 0.50 s), the mean value of the experimental data of 24.29 m.cw is lower than the value of 32.77 m.cw calculated by the 2D CFD model. These differences show the need to modify not only the components of the resolution scheme but also the geometric domain. They imply that the analysis of secondary peaks of air pocket pressure pulses resulting from an uncontrolled rapid filling process in pressurised pipelines requires individual configurations for 2D CFD models.

The greater the initial absolute pressure in the hydro-pneumatic tank, the higher air pocket pressure peak. This phenomenon can be explained in four stages (Figure 5) using results of experimental test 1. In stage 1, the first air pocket pressure is generated by the air pocket compression (Figure 6a), which is a typical behaviour presented in previous publications [14,15,19]. In stage 2, a decreasing air pocket pressure pattern occurs, due to the quantity of air expelled by the discharge orifice (Figure 6b). The second pressure peak of the air pocket is generated due to the kinetic energy of the water column blocking the orifice, as shown in stage 3 (Figure 6c), and the air pocket pressure pattern continues with some fluctuations until the water column fills the hydraulic installation completely (stage 4 in Figure 6d).

As discussed previously, the pressure variation is different for a discharge orifice compared to a standard air valve. To clearly show this behaviour, Figure 7 presents a comparison of two different air venting conditions for experimental test 1, i.e., the 7.00 mm discharge orifice and an S050 air valve (orifice size of 3.175 mm). At the beginning of the hydraulic transient, an initial pressure peak forms, with pressure magnitudes recorded as 21.7 m.cw (at 0.50 s) for the S050 air valve and 20.14 m.cw (at 0.51 s) for the discharge orifice. Figure 7 demonstrates that the pressure fluctuation for a standard air valve is more predictable by showing a typical and expected pressure variation.

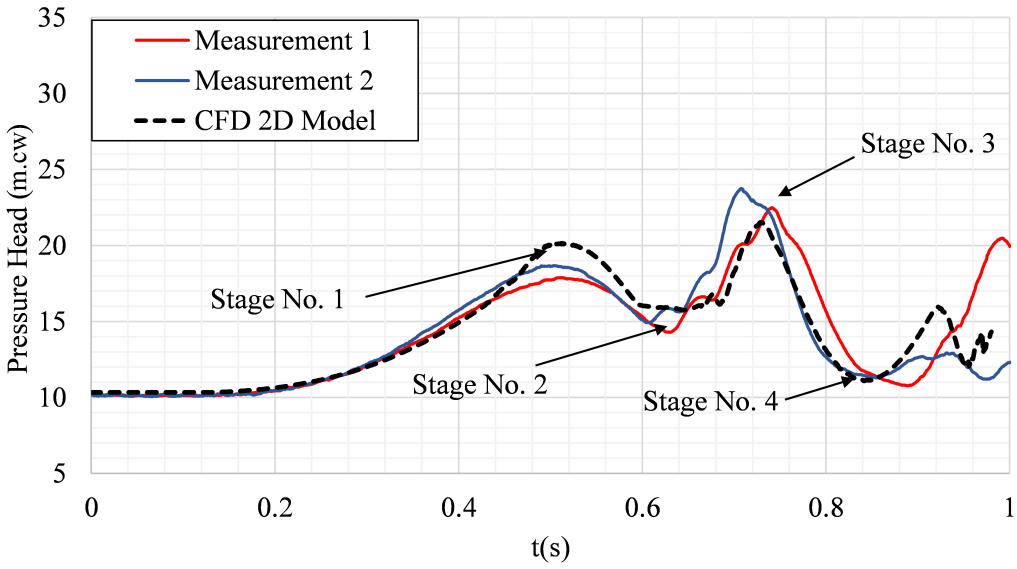

Figure 5. Conceptualisation of the uncontrolled filling process of experimental test 1.

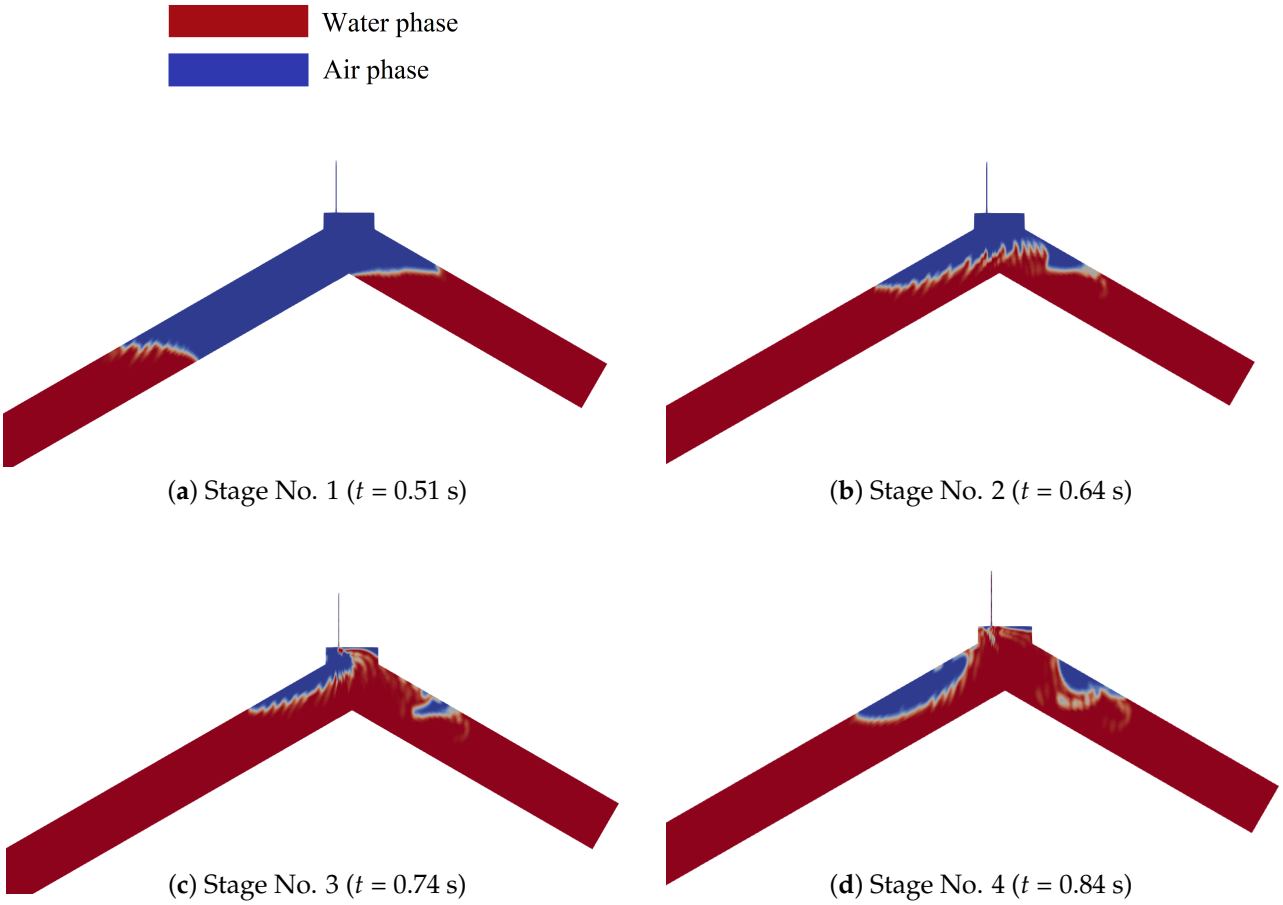

Figure 6. Air–water interface during stage 1 to 4 ocurrences for experimental test 1.

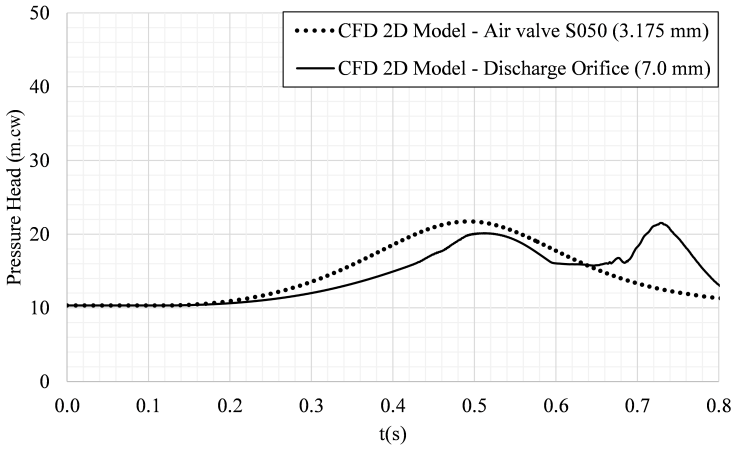

Figure 7. Comparison of air pocket pressure patterns using the S050 air valve (diameter of 3.175 mm) and the 7.0 mm discharge orifice.

Figure 8 presents water velocity patterns for experimental test 1 using the S050 air valve and the discharge orifice. According to the results, maximum water velocities for the S050 air valve ranged from 2.36 to 3.38 m/s. For the orifice discharge, water velocities varied from 2.98 to 3.88 m/s. The electro-pneumatic ball valve was completely opened at 0.12 s. An uncontrolled filling process (with the discharge orifice) showed almost no negative water velocities, while in a controlled operation (with the S050 air valve) a negative velocity zone clearly formed.

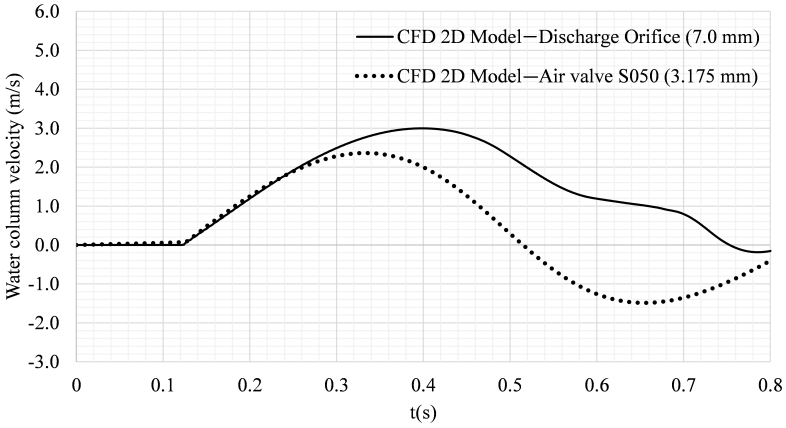

Figure 8. Comparison of water column velocity patterns using the S050 air valve (diameter of 3.175 mm) and the 7.0 mm discharge orifice.

Typically, the available studies [9,14] suggest that the greater the discharge orifice (or air valve) size, the lower the peak in air pocket pressure. This situation occurs for a controlled filling process with standard air valves installed where the kinetic energy of water columns cannot close the air venting. In that sense, the air pocket pressure behaviour using the S050 air valve has been previously studied [15,28], showing the same predicted behaviour as a standard air valve. For uncontrolled filling processes, it is not always the case that a greater orifice size results in lower air pressure values (see second peak of air pocket pressure for the orifice discharge in Figure 7).

5. Conclusions

Air valves are designed to mitigate the overpressures generated by entrapped air pockets during rapid filling processes. For controlled filling processes, the largest air valve sizes reduce the air pocket pressure peaks. However, if the kinetic energy of the water columns is enough to close the entrance of the air valves (upper part of the pipeline) with water, then a second peak of air pocket pressure is observed during uncontrolled filling operations, which can be higher than the first (controlled filling operation). In this sense, it is recommended that filling operations should be performed following the recommendations of technical manuals, or internal practices should be developed to ensure a controlled operation to prevent air pocket overpressure (undesirable second peak). Thus, the water velocity and pressure differential should be controlled during filling processes.

Two-dimensional CFD models can be used to understand uncontrolled water filling operations in hydraulic installations, which are characterised by the occurrence of two peaks in air pocket pressure. The overpressure peaks generated in hydraulic installations by water hammers at high points can reach values similar to air pocket overpressures in pipelines with air valves having a smaller orifice diameter. Future work on uncontrolled filling operations should be carried out using 3D CFD simulations.

Author Contributions: Conceptualisation, A.M.A.-M.; methodology, O.E.C.-H. and D.A.P.-V.; software, A.M.A.-M. and S.O.; validation, V.S.F.-M., H.M.R., M.B. and P.L.I.-R.; formal analysis, A.M.A.-M. and D.A.P.-V.; investigation, A.M.A.-M., D.A.P.-V. and S.O.; resources, A.M.A.-M. and O.E.C.-H.; writing—original draft preparation, A.M.A.-M. and D.A.P.-V.; writing—review and editing, O.E.C.-H., V.S.F.-M. and M.B.; supervision, O.E.C.-H. All authors have read and agreed to the published version of the manuscript.

Funding: This research received no external funding.

Conflicts of Interest: The authors declare no conflict of interest.

Abbreviations

DI	inner diameter
F_1	blending function (-)
$\mathbf{g}$	gravitational acceleration vector (m/s^2)
k	turbulence kinetic energy (m^2/m^2)
p	pressure (N/m^2)
p_{max}	maximum pressure (N/m^2)
P_i/γ_w	inlet pressure head (m.wc)
P_k	shear stress in CFD model (N/m^2)
t	time (s)
u	velocity component (m/s)
$\mathbf{u}$	velocity vector (m/s)
X_0	initial air pocket length (m)
γ	air–water volume fraction (-)
ν	mixture kinematic viscosity (m^2/s)
μ	mixture dynamic viscosity (kg/ms)
ρ	mixture density (kg/m^3)
ω	dissipation frequency (m^2/s^3)
Subscripts	
a	refers to air phase (e.g., air density)
w	refers to water phase (e.g., water dynamic viscosity)
t	refers to turbulence conditions (turbulent kinematic viscosity)
Constants of the k-ω SST model	
α_1	0.555
β^*	0.09
β_1	0.075
σ_{k1}	0.85
$\sigma_{\omega 1}$	0.50
α_2	0.44
β_2	0.0828
σ_{k2}	1.0
$\sigma_{\omega 2}$	0.856

References

1. AWWA. *Air Release, Air/Vacuum Valves and Combination Air Valves (M51)*; American Water Works Association: Denver, CO, USA, 2016.
2. Fuertes, V.S. Hydraulic Transients with Entrapped Air Pockets. Ph.D. Thesis, Department of Hydraulic Engineering, Polytechnic University of Valencia, Editorial Universitat Politècnica de València, Valencia, Spain, 2001.
3. Ramezani, L.; Karney, B.; Malekpour, A. The challenge of air valves: A selective critical literature review. *J. Water Resour. Plan. Manag.* **2015**, *141*, 04015017. [CrossRef]
4. McPherson, D.L.; Haeckler, C. *Pipelines 2012: Innovations in Design, Construction, Operations, and Maintenance, Doing More with Less*; American Society of Civil Engineers: Reston, VA, USA, 2012; pp. 983–989.
5. Liou, C.P.; Hunt, W.A. Filling of pipelines with undulating elevation profiles. *J. Hydraul. Eng.* **1996**, *122*, 534–539. [CrossRef]
6. Izquierdo, J.; Fuertes, V.S.; Cabrera, E.; Iglesias, P.L.; Garcia-Serra, J. Pipeline start-up with entrapped air. *J. Hydraul. Res.* **1999**, *37*, 579–590. [CrossRef]
7. Liu, D.; Zhou, L.; Karney, B.; Zhang, Q.; Ou, C. Rigid-plug elastic-water model for transient pipe flow with entrapped air pocket. *J. Hydraul. Res.* **2011**, *49*, 799–803. [CrossRef]
8. Zhou, L.; Liu, D.; Karney, B. Investigation of hydraulic transients of two entrapped air pockets in a water pipeline. *J. Hydraul. Eng.* **2013**, *139*, 949–959. [CrossRef]
9. Zhou, L.; Pan, T.; Wang, H.; Liu, D.; Wang, P. Rapid air expulsion through an orifice in a vertical water pipe. *J. Hydraul. Res.* **2019**, *57*, 142–149. [CrossRef]
10. Besharat, M.; Tarinejad, R.; Aalami, M.T.; Ramos, H.M. Study of a compressed air vessel for controlling the pressure surge in water networks: CFD and experimental analysis. *Water Resour. Manag.* **2016**, *30*, 2687–2702. [CrossRef]
11. Hurtado-Misal, A.D.; Hernández-Sanjuan, D.; Coronado-Hernández, O.E.; Espinoza-Román, H.; Fuertes-Miquel, V.S. Analysis of Sub-Atmospheric Pressures during Emptying of an Irregular Pipeline without an Air Valve Using a 2D CFD Model. *Water* **2021**, *13*, 2526. [CrossRef]

12. Zhou, L.; Liu, D.; Ou, C. Simulation of flow transients in a water filling pipe containing entrapped air pocket with VOF model. *Eng. Appl. Comput. Fluid Mech.* **2011**, *5*, 127–140. [CrossRef]
13. Martins, N.M.C.; Delgado, J.N.; Ramos, H.M.; Covas, D.I.C. Maximum transient pressures in a rapidly filling pipeline with entrapped air using a CFD model. *J. Hydraul. Res.* **2017**, *55*, 506–519. [CrossRef]
14. Fuertes-Miquel, V.S.; López-Jiménez, P.A.; Martínez-Solano, F.J.; López-Patiño, G. Numerical modelling of pipelines with air pockets and air valves. *Can. J. Civ. Eng.* **2016**, *43*, 1052–1061. [CrossRef]
15. Coronado-Hernández, O.E.; Besharat, M.; Fuertes-Miquel, V.S.; Ramos, H.M. Effect of a commercial air valve on the rapid filling of a single pipeline: A numerical and experimental analysis. *Water* **2019**, *11*, 1814. [CrossRef]
16. Besharat, M.; Coronado-Hernández, O.E.; Fuertes-Miquel, V.S.; Viseu, M.T.; Ramos, H.M. Backflow air and pressure analysis in emptying a pipeline containing an entrapped air pocket. *Urban Water J.* **2018**, *15*, 769–779. [CrossRef]
17. Besharat, M.; Coronado-Hernández, O.E.; Fuertes-Miquel, V.S.; Viseu, M.T.; Ramos, H.M. Computational fluid dynamics for sub-atmospheric pressure analysis in pipe drainage. *J. Hydraul. Res.* **2019**, *58*, 553–565. [CrossRef]
18. Coronado-Hernández, O.E.; Fuertes-Miquel, V.S.; Besharat, M.; Ramos, H.M. Subatmospheric pressure in a water draining pipeline with an air pocket. *Urban Water J.* **2018**, *15*, 346–352. [CrossRef]
19. Aguirre-Mendoza, A.M.; Oyuela, S.; Espinoza-Román, H.G.; Coronado-Hernández, O.E. Fuertes-Miquel, V.S. Paternina-Verona, D.A. 2D CFD Modeling of Rapid Water Filling with Air Valves Using OpenFOAM. *Water* **2021**, *13*, 3104. [CrossRef]
20. Fuertes-Miquel, V.S.; Coronado-Hernández, O.E.; Iglesias-Rey, P.L.; Mora-Meliá, D. Transient phenomena during the emptying process of a single pipe with water–air interaction. *J. Hydraul. Eng.* **2019**, *57*, 318–326. [CrossRef]
21. Zhou, L.; Cao, Y.; Karney, B.; Bergant, A.; Tijsseling, A.S.; Liu, D.; Wang, P. Expulsion of Entrapped Air in a Rapidly Filling Horizontal Pipe. *J. Hydraul. Eng.* **2020**, *146*, 04020047. [CrossRef]
22. Romero, G.; Fuertes-Miquel, V.S.; Coronado-Hernández, O.E.; Ponz-Carcelén, R.; Biel-Sanchis, F. Analysis of hydraulic transients during pipeline filling processes with air valves in large-scale installations. *Urban Water J.* **2020**, *17*, 568–575. [CrossRef]
23. Menter, F.R. Two-equation eddy-viscosity turbulence models for engineering applications. *AIAA J.* **1994**, *32*, 1598–1605. [CrossRef]
24. Wilcox, D.C. Reassessment of the scale-determining equation for advanced turbulence models. *AIAA J.* **1988**, *26*, 1299–1310. [CrossRef]
25. Launder, B.E.; Spalding, D.B. The numerical computation of turbulent flows. In *Numerical Prediction of Flow, Heat Transfer, Turbulence and Combustion*; 1983; pp. 96–116.
26. Jasak, H. OpenFOAM: Open source CFD in research and industry. *Int. J. Nav. Archit. Ocean. Eng.* **2009**, *1*, 89–94.
27. Jasak, H.; Jemcov, A.; Tukovic, Z. OpenFOAM: A C++ library for complex physics simulations. *Int. Workshop Coupled Methods Numer. Dyn.* **2007**, *1000*, 1–20.
28. Coronado-Hernández, O.E.; Fuertes-Miquel, V.S.; Besharat, M.; Ramos, H.M. Experimental and numerical analysis of a water emptying pipeline using different air valves. *Water* **2017**, *9*, 98. [CrossRef]